crystals

MDPI

Article

CO_2 and CH_2 Adsorption on Copper-Decorated Graphene: Predictions from First Principle Calculations

Oleg Lisovski, Sergei Piskunov, Dmitry Bocharov *, Yuri F. Zhukovskii †, Janis Kleperis, Ainars Knoks and Peteris Lesnicenoks

Institute of Solid State Physics, University of Latvia, Kengaraga Street 8, LV-1063 Riga, Latvia; Olegs.Lisovskis@cfi.lu.lv (O.L.); piskunov@cfi.lu.lv (S.P.); janis.kleperis@cfi.lu.lv (J.K.); ainars.knoks@cfi.lu.lv (A.K.); Peteris.Lesnicenoks@cfi.lu.lv (P.L.)

* Correspondence: bocharov@cfi.lu.lv

† Deceased.

Abstract: Single-layer graphene decorated with monodisperse copper nanoparticles can support the size and mass-dependent catalysis of the selective electrochemical reduction of CO_2 to ethylene (C_2H_4). In this study, various active adsorption sites of nanostructured Cu-decorated graphene have been calculated by using density functional theory to provide insight into its catalytic activity toward carbon dioxide electroreduction. Based on the results of our calculations, an enhanced adsorption of the CO_2 molecule and CH_2 counterpart placed atop of Cu-decorated graphene compared to adsorption at pristine Cu metal surfaces was predicted. This approach explains experimental observations for carbon-based catalysts that were found to be promising for the two-electron reduction reaction of CO_2 to CO and, further, to ethylene. Active adsorption sites that lead to a better catalytic activity of Cu-decorated graphene, with respect to general copper catalysts, were identified. The atomic configuration of the most selective CO_2 toward the reduction reaction nanostructured catalyst is suggested.

Keywords: graphene; nanodecoration; first-principles calculations; adsorption; CO_2 electroreduction

Citation: Lisovski, O.; Bocharov, D.; Piskunov, S.; Zhukovskii, Y.F.; Kleperis, J.; Knoks, A.; Lesnicenoks, P. CO_2 and CH_2 Adsorption on Copper-Decorated Graphene: Predictions from First Principle Calculations. *Crystals* **2022**, *12*, 194. https://doi.org/10.3390/cryst12020194

Academic Editors: Walid M. Daoush, Fawad Inam, Mostafa Ghasemi Baboli and Maha M. Khayyat

Received: 12 November 2021
Accepted: 25 January 2022
Published: 28 January 2022

1. Introduction

The electroreduction of CO_2 from exhausts to hydrocarbons can provide a sustainable supply of valuable raw materials for the chemical industry and fuels for transport and energetics [1]. The reduction of captured excessive carbon dioxide from the atmosphere could lead to a decrease in the greenhouse effect. CO_2 can be reduced to hydrocarbons—in particular, ethylene and methane (CH_4)—by electrochemical reactions $2CO_2 + 12e^- + 8H_2O \rightarrow C_2H_4 + 12OH^-$ and $CO_2 + 8e^- + 6H_2O \rightarrow CH_4 + 8OH^-$, respectively. Ethylene has a wide range of applications in industry, polymer production, and agriculture. One of the most promising catalysts that can electroreduce CO_2 to C_2H_4 is copper metal [2,3]. However, along with ethylene (C_2H_4), many other carbon side-products are formed, including methane (CH_4), carbon monoxide (CO), and formate anion ($HCOO^-$) [4–7]. Besides, copper catalysts are very susceptible to poisoning and deactivation, usually, within half an hour after the start of the reduction process of carbon dioxide [8,9]. For the aforementioned reasons, significant efforts have recently been made to develop catalysts that can selectively reduce CO_2 to ethylene over long-lasting time periods. [7,10,11]. Polycrystalline Cu surfaces do not show a significant preference towards ethylene formation, with a C_2H_4/CH_4 product ratio of around 1:2 [3–5,12,13]. Their insufficient selectivity is considered to be due to the large heterogeneity of the centers of different catalytic activities on the polycrystalline surface. This is confirmed by the study of the influence of different copper planes on the selectivity of the electroreduction of carbon dioxide [7,14]. It was found that the (100) surface of single crystals of Cu favors the formation of ethylene more than Cu (111), as indicated by their ratios C_2H_4/CH_4 1.3 and 0.2, respectively [7]. Interestingly, when the high index Cu (711), Cu (911), and Cu (810) planes formed by cleaving Cu (100) were

examined, an even higher selectivity was displayed toward C_2H_4, with the C_2H_4/CH_4 ratio increasing to 10 for Cu (711). The reason for the catalyst's selectivity toward certain hydrocarbons is the increased number of surface steps in the high index facets or periodic formation of Cu terraces. This means that the system that is modified in such a way may exhibit an increased efficiency.

It was shown that copper nanoparticles with a large surface area have good selectivity for the formation of hydrocarbons, especially of ethylene [6]. It has been suggested that the edges and numerous steps formed on the surface of copper nanoparticles may be of decisive importance for the selective formation of ethylene. In favor of this, quantum chemical modeling has shown that intermediate reaction products, such as $^*CHO$, are more stable at the steps of the Cu (211) surface than at the Cu (100) terraces. (Hereafter, an asterisk indicates that a species is adsorbed on a surface). This can lead to an increase in their concentration, and, ultimately dimerization to C_2H_4 [15].

Composites and hybrid structures, as well as nanoobjects based on graphene, has attracted huge attention in experimental and theoretical studies during the last decade [16–22] after this material was discovered in 2004 by Novoselov and Geim [23]. The decoration of graphene with metals (e.g., Fe [24], Pt [25,26], Pd [27]), as well as organic (e.g., tetracyanoethylene [28]) and inorganic compounds (e.g., Bi_2O_3 [29]), could improve electrocatalytic adsorption and gas sensing properties toward different gases

Different graphene-based catalysts for direct electrochemical CO_2 reduction were reported in the literature, e.g., atomic Fe dispersed on nitrogen-doped graphene [30], B-doped graphene [31], N-doped graphene [32], defective graphene produced by a nitrogen removal procedure from N-doped graphene [33], Ni-decorated graphene [34], Co_3O_4 spinel nanocubes on N-doped graphene [35], etc. The review of graphene-based materials for electrochemical CO_2 reduction was published by Ma et al. recently [36]. Several recent studies show that the modification of the graphene surface by copper nanoparticles or by creating Cu-contained heterostructures is an interesting approach in the development of efficient electrocatalysts [37–51] .

These preceding studies have led us to elaborate on a theoretical model for a stable C_2H_4-selective electrocatalyst based on copper-nanocluster-decorated graphene and to understand how this selectivity can be increased. Carbon-based materials are potentially interesting catalysts for the CO_2 reduction reaction due to their low cost and especially due to their ability to form a wide range of hybrid nanostructures [52–57]. Carbon-based catalysts are chemically inactive at negative bias potentials and provide high overpotentials for the hydrogen evolution reaction compared to metal surfaces [58]. Pristine graphene does not exhibit any catalytic activity. However, by introducing dopants [59–61] and defects [62] during the synthesis, the electronic structure and catalytic properties of nanostructured carbon materials [62] are tailored. In particular, N-doping has been shown to significantly enhance the CO_2 reduction activity [39,41,61,63–66].

Experimental results obtained recently [67] suggest that the reaction pathways of the CH_4 and C_2H_4 formation are separated at an early stage of CO reduction. Results from a recent experimental study of CO electroreduction on single-crystal copper electrodes [68] imply that there are two separate pathways for C_2H_4 formation: one (i) that shares an intermediate with the pathway to CH_4, and a second one (ii) that occurs mainly on Cu (100) and probably involves the formation of a CO dimer as the key intermediate [69]. Considering the pathway (i), it is obvious that the $^*CH_2$ dimerization is a crucial step for the final C_2H_4 production (the so-called "carbene" mechanism). $^*CH_2$ can be produced by the protonation and deoxygenation of $^*CO$ [5]. $^*CH_2$ can be also obtained from subsequent reductions of $^*HCO$, $^*C$, and $^*CH$. The further reduction of a single $^*CH_2$ gives rise to $^*CH_3$ and finally to CH_4.

In this study, the adsorption of CO_2 is considered to typically be the rate-determining step in the CO_2 reduction reaction, and thus it is desirable to find/design catalyst sites that bond CO_2 strongly—preferably stronger than H adsorption [70]. To shed light on the trends in the catalytic activity of the Cu-decorated pristine and N-doped graphene system, in this work, systematic density functional theory (DFT) calculations of the adsorption of CO_2 and

intermediates on Cu-decorated graphene are performed. The first principle calculations is performed for the monodisperse Cu_7 nanocluster deposited at the 5 × 5 supercell of graphene to predict the electronic properties of the Cu_7 facet in light of its different affinities for $^*CO_2$ and $^*CH_2$, and thus to provide deeper insights into its intrinsic activities for CO_2 electroreduction. The reaction energies for the formation of intermediates on Cu_7/graphene-nanostructured surfaces have been calculated using the hybrid DFT approach. In general, this work may not only give a deep insight into the reaction mechanisms toward C_2H_4 formation on Cu-decorated carbon nanomaterials, but may also provide guidelines for designing Cu-based catalysts to effectively produce multicarbon compounds.

2. Computational Details

Modeling was carried out at the DFT level of theory. This approach is based on the linear combination of atomic orbitals (LCAO) method with atom-centered localized Gaussian-type functions (GTFs) forming the basis sets (BS). Fully relaxed Cu_7/graphene nanostructures were calculated using hybrid exchange-correlation functional HSE06 according to the prescription given in Refs. [71,72]. Its particular feature is the use of an error-function-screened Coulomb potential for calculating the exchange energy. This functional was chosen to reproduce the basic atomic and electronic properties of both graphene and the most stable Cu (111) qualitatively close to those experimentally observed. The calculations were executed with CRYSTAL17 computational code [73], which was developed for the atomistic modeling of solid state chemistry. Using such a computation strategy, the geometries have been optimized with various species adsorbed on the graphene and metal Cu catalyst, and the adsorption energies of various species that are considered in this study have been calculated for nitrogen, oxygen, the CO_2 molecule, and the CH_2 radical. Besides the graphene and copper catalyst, basis sets are required for atoms of adsorbed species. For all atoms in the studied materials, full electron valence BSs [73] were used. For Cu, C, O, and H atoms, the triple-zeta BSs were obtained from Ref. [74]; on the other side, for the N atom, the basis set in the form of 6s-31sp-1d was obtained from Ref. [75].

To evaluate the Coulomb and exchange series appearing in the SCF equations for periodic systems, five tolerances were controlled: 10^{-8}, 10^{-8}, 10^{-8}, 10^{-8}, 10^{-16} (related to estimates of overlap or penetration for integrals of Gaussian functions on different centers, which define cut-off limits for series summation). To provide the correct summation in both direct and reciprocal lattices, the reciprocal space was integrated by sampling the interface Brillouin zone (BZ) with the 8 × 8 × 1 Monkhorst–Pack meshes [76] for slab calculations, which gives, in total, 34 k-points evenly distributed in the BZ. The calculations are considered to be convergent if the total energy differs by 10^{-7} a.u. or less in two successive cycles of the self-consistent-field (SCF) procedure [73].

The adsorption energy E_{ads} was calculated with the following equation:

$$E_{ads} = E_{ads/sub} - E_{molecule} - E_{sub} \quad (1)$$

where $E_{ads/sub}$ and E_{sub} are the total energy of the Cu_7/graphene nanostructure with the adsorbed CO_2, molecule or $^*CH_2$ intermediate, and Cu_7/graphene nanostructure slab, respectively, and $E_{molecule}$ is the total energy of the isolated CO_2 molecule or $^*CH_2$ intermediate, analogously to Ref. [77]. The energetically favorable adsorption (chemisorption) takes place if the adsorption energy E_{ads} is negative [78].

3. Results and Discussion

3.1. Cu/Graphene Cluster

Within the framework of this study, an efficient and reliable model of the monodisperse Cu_7 cluster deposited on single-layered graphene is constructed. The model consists of a 5 × 5 graphene supercell periodically repeated in the *xy* plane, with seven Cu atoms forming a nanodot deposited in every supercell. Such a model is a balanced solution for the efficient use of computer resources and reliable prediction of the electronic structure and energetics of the nanostructures under study. Figure 1 shows schematic views (aside and

atop) for the fully optimized two-dimensional Cu_7/graphene nanostructure containing the faceted Cu nanodot. For this cluster, a complete relaxation of the atomic coordinates was carried out and the binding energy of Cu atoms was estimated for this model.

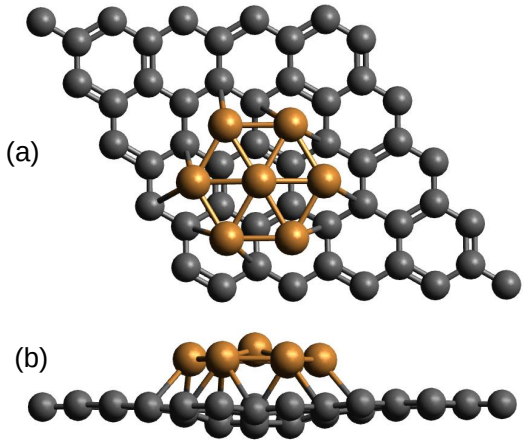

Figure 1. Top (**a**) and aside (**b**) views of equilibrium structure of six-faceted Cu nanopyramid deposited on graphene monolayer. Grey balls stand for carbon atoms and orange for copper.

The Cu_7 cluster is quite strongly physisorbed to the graphene layer with the binding energy of −1.54 eV/Cu atom. The negative binding energy means that energy is released after the substrate–adsorbate coupling. Single Cu atoms tend to adsorb at the hollow sites of graphene with the binding energy of −2.65 eV/Cu atom. Thus, Cu atoms deposited at graphene could reproduce the facets of the most stable Cu (111) surface. Nevertheless, a single Cu atom deposited at graphene forms quite weak Cu-C graphene bonds, with a bond population of 80 milli electrons.

The strongest bonding between Cu and graphene takes place at the defective graphene layer containing a carbon vacancy (Figure 2). The binding energy of the Cu-$C_{vacancy}$ complex is approximately −6.63 eV/Cu atom. However, the energy of vacancy formation is quite high (17.5 eV) and such a mechanism of Cu cluster adsorption at graphene is energetically unfavorable.

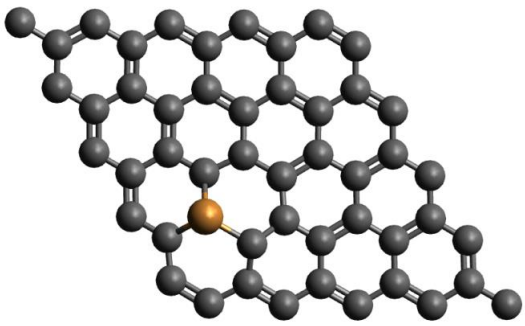

Figure 2. Equilibrium structure of $C_{graphene}$ atom substituted for Cu with the binding energy of −3.59 eV/Cu atom. Grey balls stand for carbon atoms and orange for copper.

Since the N-doping has been shown to significantly enhance the CO_2 reduction activity of graphene [39,41,61,63–66], the six-faceted Cu nanopyramid deposited atop the N-saturated graphene monolayer (Figure 3) is considered as well. The presence of the nitrogen atoms at the graphene support allows for the strong chemisorption of the Cu atom with the bond population of Cu–N = 303 milli electrons and N–$C_{graphene}$ = 344 milli electrons. The presence of a nitrogen monolayer may lead to a stronger adsorption of the Cu nanocluster at graphene; however, the presence of N practically does not influence CO_2 adsorption at Cu_7/graphene. Therefore, an N layer atop graphene is not considered in the further modeling of CO_2 reduction.

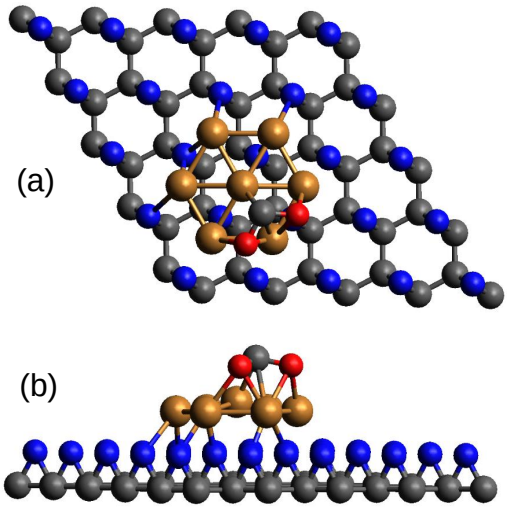

Figure 3. Schematic representation of top (**a**) and aside (**b**) views of six-faceted Cu nanopyramid deposited on N-saturated graphene monolayer. Grey balls stand for carbon atoms, orange for copper, red balls are oxygen atoms, and blue ones are nitrogen atoms.

Due to the relatively large distance between carbon layers in double-layered graphene (∼6.94 Å), the layer-to-layer interaction is negligible and does not influence the Cu nanocluster adhesion to the graphene layer. Therefore, in further modeling, it is assumed that the Cu cluster deposited at single-layered graphene can mimic the Cu cluster deposited at double-layered graphene.

Therefore, the constructed model of the six-faceted Cu nanopyramid deposited on the graphene monolayer (Figure 1) is considered as the most appropriate for large-scale ab initio total energy calculations of CO_2 and CH_2 molecules atop periodic Cu_7/graphene nanostructures (an electrically neutral system) using state-of-the-art total energy codes to estimate the energetics of a chain of elemental reactions under the influence of the copper nanocatalyst and graphene support.

3.2. CO_2 Adsorption

Taking into account that the adsorption of CO_2 is typically assumed to be the rate-determining step in CO_2 reduction, we pay major attention to the free energies of CO_2 adsorption at the Cu_7/graphene nanostructure, and, for comparative reasons, we have modeled CO_2 adsorption on its constituents, the most stable Cu (111) surface, represented by a three-layer and six-layer slab and pristine graphene (Figure 4). For the slabs, we considered the non-symmetrical one-sided and symmetrical two-sided deposition of absorbed CO_2 molecules. The adsorption energies for the CO_2 molecule and $^*CH_2$ intermediate for the Cu_7/graphene nanostructure, the Cu (111) surface, represented by the three-layer and six-layer slab and pristine graphene, are given in Table 1.

Table 1. Calculated adsorption energies (eV) of CO_2 molecule and $^*CH_2$ intermediate on Cu_7/graphene nanostructure, Cu (111) surface, represented as three-layer and six-layer slab, and pristine graphene layer with 5 × 5 supercell.

		CO_2	$^*CH_2$
Cu_7/graphene		−6.04	−7.31
three-layer slab	one-sided	−6.69	−6.53
	two-sided	−6.74	−6.43
six-layer slab	one-sided	−6.99	−6.38
	two-sided	−6.89	−6.46
pristine graphene		−0.43	−3.12

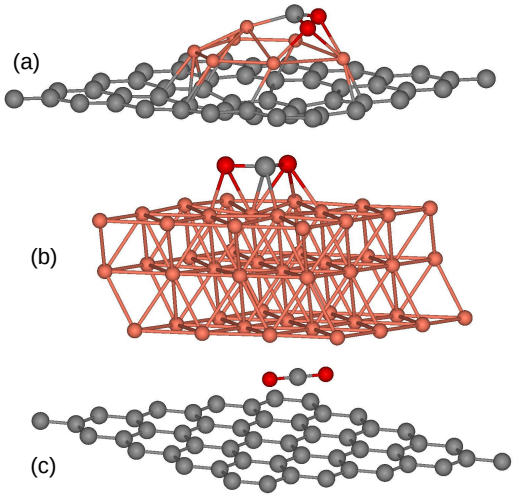

Figure 4. Schematic representation of the most energetically favorable adsorption positions of CO_2 molecule on (**a**) Cu_7/graphene nanostructure, (**b**) Cu (111) surface, and (**c**) pristine graphene monolayer. Grey balls stand for carbon atoms, orange for copper, and red balls are oxygen.

For all materials under consideration, the most energetically favourable adsorption site for the CO_2 molecule is the bridge position. Only the weak physisorption of CO_2 on pristine graphene is predicted from our calculation, with a relatively small free adsorption energy of −0.43 eV, which is in agreement with trends reported in Ref. [28]. The free adsorption energy calculated for the Cu (111) surface is in the range between −6.69 and −6.99 eV depending on the slab thickness and one-sided or two-sided adsorption of CO_2 molecules, whereas the adsorption energy of −6.04 eV per CO_2 molecule is predicted for the Cu_7/graphene nanostructure. A lower number points to a stronger chemical binding. The stronger binding of CO_2 to the Cu_7 nanocluster at graphene (similar to the adsorption at the pristine Cu (111) surface) can be explained by the presence of <111> grain boundaries of the Cu_7 nanocluster, which are known to be chemically more reactive. Figure 5a shows the projected density of states (PDOS) calculated for the CO_2 molecule adsorbed at the Cu (111) surface. The strong adsorption of the CO_2 molecule can be explained by Cu 3*d*–O 2*p* orbitals hybridization seen in Figure 5a by the peaks at approximately −4 eV. The Cu–O bond population calculated by Mulliken population analysis is equal to 434 milli electrons. Both O atoms of the CO_2 molecule are strongly bonded to the Cu atoms of the Cu (111) surface. The only weak physisorption of CO_2 is predicted at graphene (PDOS in Figure 5b), with a $C_{graphene}$–C_{CO_2} bond population of 0.012 milli electrons Our prediction is in agreement with the recent experimental observations. According to the data available in the literature, to improve the selectivity of CO_2 electrochemical reduction in producing C_2 products, Kanan et al. synthesized Cu nanoparticles containing grain boundaries and observed a substantial enhancement in the Faradaic efficiency of generating multi-carbon hydrocarbons [79]. This enhancement is correlated with the density of the grain boundary areas [80]. Cheng et al. conducted the atomistic modeling for the chemical vapor deposition process of Cu nanoparticles and found that strong CO binding with under-coordinated surface square sites could promote C–C coupling ("carbene" mechanism) [81]. According to our predictions, the boundary between the Cu_7 cluster and graphene can demonstrate the best catalytic ability for the C_2H_4 formation. This is due to the adsorption properties of neighboring Cu sites that are significantly perturbed by the presence of the nearest C, and the stronger Cu–O bonding is formed on the catalyst surface, which can also enhance $H_2C{=}CH_2$ evolution [14].

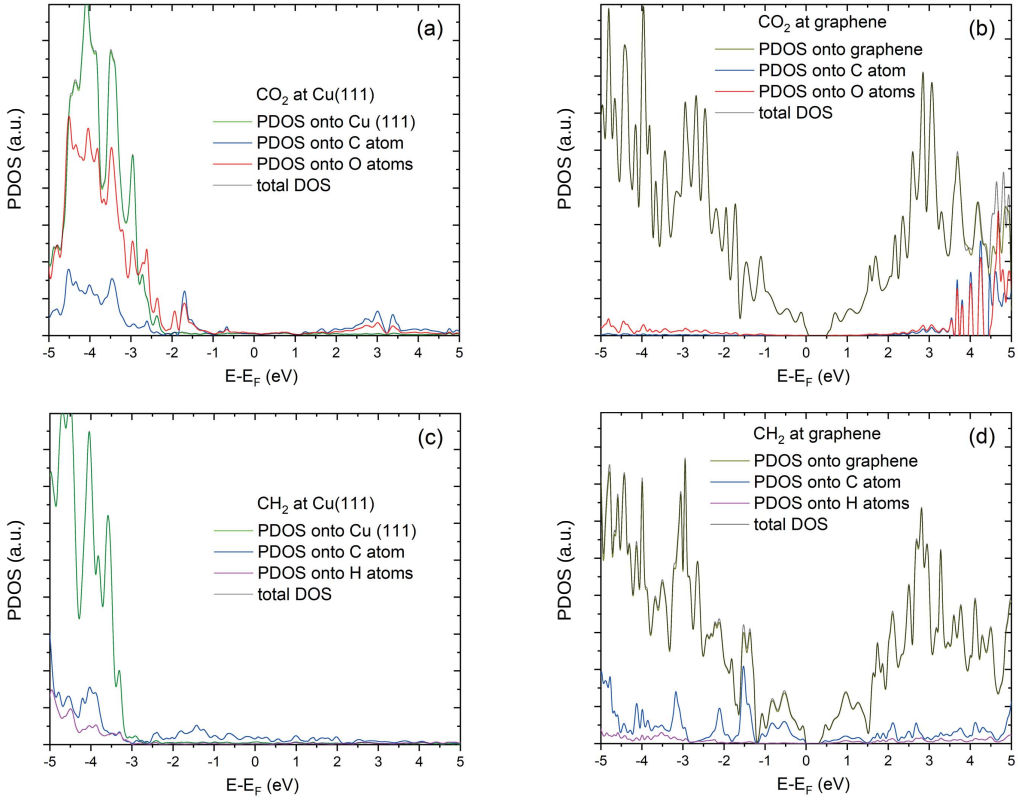

Figure 5. Projected density of states (PDOS) calculated for (**a**) CO_2 adsorbed at Cu (111) surface, (**b**) CO_2 adsorbed at graphene, (**c**) CH_2 adsorbed at Cu (111) surface, and (**d**) CH_2 adsorbed at graphene. PDOS onto all orbitals of H, C, and O atoms are magnified 10 times.

3.3. CH_2 Adsorption

Results from a recent experimental study of CO electroreduction on single-crystal copper electrodes [5] further implied that one of the most probable pathways for C_2H_4 formation is one that shares an intermediate with the pathway to CH_4. Considering that pathway, it is reasonable that the $^*CH_2$ dimerization is a crucial step for the final C_2H_4 production ("carbene" mechanism). The further reduction of single $^*CH_2$ gives rise to $^*CH_3$ and finally to CH_4. Therefore, in this study, the adsorption energy of $^*CH_2$ on Cu_7/graphene, pristine Cu (111), and pristine graphene (Figure 6) is calculated. For both pristine Cu (111) and Cu_7/graphene nanostructures, the most energetically favorable adsorption site of $^*CH_2$ adsorbate is the hollow position between neighboring copper atoms, whereas the bridge position between neighboring C–C atoms is the most energetically preferable for the $^*CH_2$ adsorption on pristine graphene. Figures 5c,d show the PDOS calculated for the CH_2 component adsorbed on the Cu (111) surface and graphene, respectively. CH_2 relatively strongly adsorbed at Cu (111) with hybrydized Cu 3*d*–C 2*p* orbitals, forming square planar sp^2d hybridisation (Figure 5c, peaks at approximately −4 eV) and a Cu–C bond population of 390 milli electrons, whereas the $C_{graphene}$–C_{CH_2} bond population of 0.240 milli electrons is calculated for CH_2 at graphene.

Only a weak physisorption of $^*CH_2$ on pristine graphene is predicted from our calculation, with a relatively small adsorption energy of −3.12 eV (PDOS in Figure 5d), which is in qualitative agreement with the observation reported in Ref. [28]. This may consequently lead to the relatively small barrier of CH_2–CH_2 dimerization. The adsorption energy calculated for the Cu (111) surface is in the range between −6.38 and −6.53 eV for the different thicknesses of slabs and the symmetrical/non-symmetrical deposition of $^*CH_2$ intermediates, whereas a free adsorption energy of −7.31 eV is predicted for the Cu_7/graphene nanostructure (Table 1). From the calculated adsorption energies, we predict that the most energetically preferable CH_2 dimerization can take place on pristine graphene,

whereas only a small difference in CH_2 dimerization can be predicted for the Cu (111) and Cu_7/graphene nanocluster.

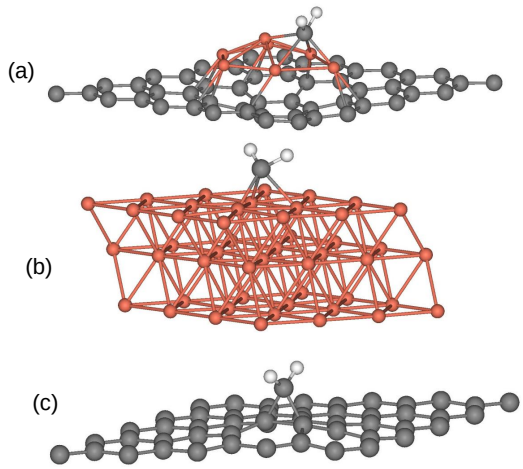

Figure 6. Schematic representation of the most energetically favourable adsorption positions of $^*CH_2$ intermediate on the top of (**a**) Cu_7/graphene nanostructure, (**b**) Cu (111) surface, and (**c**) pristine graphene monolayer. Grey balls stand for carbon atoms, orange for copper, and white balls are hydrogen.

4. Conclusions

The main goal of this study is to contribute to the description of experimentally achievable results, allowing for the further optimization of the cathode composition and structure. In order to give theoretical predictions, we have constructed an efficient and reliable model that can be considered as the most appropriate for large-scale ab initio total energy calculations of CO_2 and CH_2 elements atop periodic Cu_7/graphene nanostructures. In these calculations, in order to examine a chain of elemental reactions under the influence of the copper nanocatalyst and graphene support, the state-of-the-art total energy codes were used. In the modeled nanocluster, Cu atoms reproduce the facets of the most stable Cu (111) surface. Adatoms and/or defects, e.g., vacancies, at the graphene support may make Cu–C graphene bonds stronger, facilitating the growth of the nanocluster. Assuming that the adsorption of CO_2 is typically the rate-determining step in the CO_2 reduction reaction, the energies of CO_2 adsorption at the Cu_7/graphene nanostructure have been calculated and compared to the adsorption energies of species placed on the pristine Cu (111) surface and pristine graphene. The strong binding of CO_2 to the Cu_7 nanocluster at graphene is close to binding to the pristine Cu (111) surface. This is explained by the presence of <111> facets at the Cu_7 nanocluster. This prediction is in agreement with the recent experimental observations to improve the selectivity of CO_2 electrochemical reduction in producing the CH_2–CH_2 intermediates. Cu nanoparticles containing grain boundaries were synthesized and a substantial enhancement in the Faradaic efficiency of generating multi-carbon hydrocarbons was observed [79]. This enhancement is correlated with the density of the grain boundary areas [80]. According to predictions obtained in this study, the Cu cluster at graphene demonstrates the best catalytic ability for C_2H_4 formation. This is due to the fact that the adsorption properties of neighboring Cu sites are significantly perturbed by the presence of the nearest C, and the stronger Cu–O bonding is formed on the catalyst surface, which also can enhance $H_2C{=}CH_2$ evolution. Based on this, it is predicted that the larger the length of the grain boundaries of the Cu_n nanocluster deposited at graphene, the more selective the catalyst is to the C_2H_4. According to a recent experimental study of CO_2 electroreduction on copper electrodes [81], it is expected that one of the most probable pathways for C_2H_4 formation is one that shares an intermediate with the pathway to CH_4. Considering this pathway, it is obvious that $^*CH_2$ dimerization is a crucial step for the final C_2H_4 production ("carbene" mechanism). In this respect, the CH_2–CH_2 dimerization reaction is responsible for the C_2H_4 evolution. The lowest dimerization

barrier can be predicted for the pristine graphene due to the lowest adsorption energy, meaning that the whole CO_2 reduction reaction taking place at the grain boundary of the Cu_n/graphene nanocluster may lead to an improved selectivity to ethylene.

Author Contributions: O.L.: conceptualization, investigation, methodology, visualization, formal analysis, writing—review and editing; S.P.: conceptualization, investigation, methodology, formal analysis, writing—original draft, writing—review and editing; D.B.: investigation, resources, formal analysis, writing—original draft, writing—review and editing; Y.F.Z.: conceptualization, supervision; J.K.: conceptualization, funding acquisition, project administration, writing—review and editing, supervision; A.K.: conceptualization, investigation, writing—review and editing; P.L.: conceptualization, investigation. All authors have read and agreed to the published version of the manuscript.

Funding: The authors would like to express their gratitude for funding from the European Union's Horizon 2020 research and innovation programme under grant agreement No. 768789 (CO2EXIDE project). In the last stage of investigation and during the preparation of the publication, the authors were assisted by the postdoc D.B. with his own funding from project No. 1.1.1.2/VIAA/l/16/147 (1.1.1.2/16/I/001) under the activity "Post-doctoral research aid" realized at the Institute of Solid State Physics, University of Latvia.

Institutional Review Board Statement: Not applicable.

Informed Consent Statement: Not applicable.

Data Availability Statement: The data presented in this study are available in article.

Acknowledgments: Calculations were performed using Latvian Super Cluster (LASC), located in Center of Excellence at Institute of Solid State Physics, the University of Latvia, which is supported by European Union Horizon2020 Framework Programme H2020-WIDESPREAD-01-2016-2017-TeamingPhase2 under Grant Agreement No. 739508, project CAMART2.

Conflicts of Interest: The authors declare no conflict of interest. The funders had no role in the design of the study; in the collection, analyses, or interpretation of data; in the writing of the manuscript, or in the decision to publish the results.

References

1. Whipple, D.T.; Kenis, P.J.A. Prospects of CO_2 utilization via direct heterogeneous electrochemical reduction. *J. Phys. Chem.* **2010**, *1*, 3451–3458. [CrossRef]
2. Hori, Y.; Wakebe, H.; Tsukamoto, T.; Koga, O. Electrocatalytic process of CO selectivity in electrochemical reduction of CO_2 at metal electrodes in aqueous media. *Electrochim. Acta* **1994**, *39*, 1833–1839. [CrossRef]
3. Hori, Y. Electrochemical CO_2 reduction on metal electrodes. In *Modern Aspects of Electrochemistry*; Vayenas C., White, R., Gamboa-Aldeco, M., Eds.; Springer: New York, NY, USA, 2008; pp. 89–189.
4. Kuhl, K.P.; Cave, E.R.; Abram, D.N.; Jaramillo, T.F. New insights into the electrochemical reduction of carbon dioxide on metallic copper surfaces. *Energy Environ. Sci.* **2012**, *5*, 7050–7059. [CrossRef]
5. Hori, Y.; Murata, A.; Takahashi, R. Formation of hydrocarbons in the electrochemical reduction of carbon dioxide at a copper electrode in aqueous solution. *J. Chem. Soc. Faraday Trans. 1* **1989**, *85*, 2309–2326. [CrossRef]
6. Tang, W.; Peterson, A.A.; Varela, A.S.; Jovanov, Z.P.; Bech, L.; Durand, W.J.; Dahl, S.; Nørskov, J.K.; Chorkendorff, I. The importance of surface morphology in controlling the selectivity of polycrystalline copper for CO_2 electroreduction. *Phys. Chem. Chem. Phys.* **2012**, *14*, 76–81. [CrossRef]
7. Hori, Y.; Takahashi, I.; Koga, O.; Hoshi, N. Electrochemical reduction of carbon dioxide at various series of copper single crystal electrodes. *J. Mol. Catal. Chem.* **2003**, *199*, 39–47. [CrossRef]
8. Hori, Y.; Konishi, H.; Futamura, T.; Murata, A.; Koga, O.; Sakurai, H.; Oguma, K. Deactivation of copper electrode in electrochemical reduction of CO_2. *Electrochim. Acta* **2005**, *50*, 5354–5369. [CrossRef]
9. DeWulf, D.W.; Jin, T.; Bard, A.J. Electrochemical and surface studies of carbon dioxide reduction to methane and ethylene at copper electrodes in aqueous solutions. *J. Electrochem. Soc.* **1989**, *136*, 1686–1691. [CrossRef]
10. Schouten, K.J.P.; Pérez Gallent, E.; Koper, M.T. The influence of pH on the reduction of CO and CO_2 to hydrocarbons on copper electrodes. *J. Electrochem. Soc.* **2014**, *716*, 53–57. [CrossRef]
11. Schouten, K.J.P.; Pérez Gallent, E.; Koper, M.T.M. Structure sensitivity of the electrochemical reduction of carbon monoxide on copper single crystals. *ACS Catal.* **2013**, *3*, 1292–1295. [CrossRef]
12. Li, C.W.; Kanan, M.W. CO_2 reduction at low overpotential on Cu electrodes resulting from the reduction of thick Cu_2O films. *J. Am. Chem. Soc.* **2012**, *134*, 7231–7234. [CrossRef] [PubMed]
13. Gattrell, M.; Gupta, N.; Co, A. A review of the aqueous electrochemical reduction of CO_2 to hydrocarbons at copper. *J. Electroanal. Chem.* **2006**, *594*, 1–19. [CrossRef]

14. Hori, Y.; Takahashi, I.; Koga, O.; Hoshi, N. Selective formation of C2 compounds from electrochemical reduction of CO_2 at a series of copper single crystal electrodes. *J. Phys. Chem. B* **2002**, *106*, 15–17. [CrossRef]
15. Durand, W.J.; Peterson, A.A.; Studt, F.; Abild-Pedersen, F.; Nørskov, J.K. Structure effects on the energetics of the electrochemical reduction of CO_2 by copper surfaces. *Surf. Sci.* **2011**, *605*, 1354–1359. [CrossRef]
16. Fu, P.; Jia, R.; Wang, J.; Eglitis, R.I.; Zhang, H. 3D-graphene/boron nitride-stacking material: A fundamental van der Waals heterostructure. *Chem. Res. Chin. Univ* . **2018**, *34*, 434–439. [CrossRef]
17. Sergeyev, D.; Ashikov, N.; Zhanturina, N. Electric transport properties of a model nanojunction "Graphene–Fullerene C_{60}–Graphene". *Int. J. Nanosci.* **2021**, *20*, 2150007, [CrossRef]
18. Krasnenko, V.; Kikas, J.; Brik, M.G. Modification of the structural and electronic properties of graphene by the benzene molecule adsorption. *Phys. B Condens. Matter* **2012**, *407*, 4557–4561. [CrossRef]
19. Krasnenko, V.; Boltrushko, V.; Hizhnyakov, V. Vibronic interactions proceeding from combined analytical and numerical considerations: Covalent functionalization of graphene by benzene, distortions, electronic transitions. *J. Chem. Phys.* **2016**, *144*, 134708, [CrossRef]
20. Krasnenko, V.; Boltrushko, V.; Klopov, M.; Hizhnyakov, V. Conjoined structures of carbon nanotubes and graphene nanoribbons. *Phys. Scr.* **2014**, *89*, 044008, [CrossRef]
21. Bystrov, V.S.; Bdikin, I.K.; Silibin, M.V.; Meng, X.J.; Lin, T.; Wang, J.L.; Karpinsky, D.V.; Bystrova, A.V.; Paramonova, E.V. Pyroelectric properties of ferroelectric composites based on polyvinylidene fluoride (PVDF) with graphene and graphene oxide. *Ferroelectrics* **2019**, *541*, 17–24. [CrossRef]
22. Xi, J.Y.; Jia, R.; Li, W.; Wang, J.; Bai, F.Q.; Eglitis, R.I.; Zhang, H.X. How does graphene enhance the photoelectric conversion efficiency of dye sensitized solar cells? An insight from a theoretical perspective. *J. Mater. Chem. A* **2019**, *7*, 2730–2740. [CrossRef]
23. Novoselov, K.S.; Geim, A.K.; Morozov, S.V.; Jiang, D.; Zhang, Y.; Dubonos, S.V.; Grigorieva, I.V.; Firsov, A.A. Electric field effect in atomically thin carbon films. *Science* **2004**, *306*, 666–669. [CrossRef] [PubMed]
24. Ali, M.; Tit, N.; Yamani, Z.H. First principles study on the functionalization of graphene with Fe catalyst for the detection of CO_2: Effect of catalyst clustering. *Appl. Surf. Sci.* **2020**, *502*, 144153. [CrossRef]
25. Salih, E.; Ayesh, A.I. Pt-doped armchair graphene nanoribbon as a promising gas sensor for CO and CO_2: DFT study. *Phys. E Low-Dimens. Syst. Nanostruct.* **2021**, *125*, 114418. [CrossRef]
26. Rad, A.S. Adsorption of C_2H_2 and C_2H_4 on Pt-decorated graphene nanostructure: Ab-initio study. *Synth. Met.* **2016**, *211*, 115–120. [CrossRef]
27. Ma, L.; Zhang, J.M.; Xu, K.W.; Ji, V. A first-principles study on gas sensing properties of graphene and Pd-doped graphene. *Appl. Surf. Sci.* **2015**, *343*, 121–127. [CrossRef]
28. Osouleddini, N.; Rastegar, S.F. DFT study of the CO_2 and CH_4 assisted adsorption on the surface of graphene. *J. Electron Spectrosc. Relat. Phenom.* **2019**, *232*, 105–110. [CrossRef]
29. Mulik, B.B.; Bankar, B.D.; Munde, A.V.; Biradar, A.V.; Sathe, B.R. Bismuth-oxide-decorated graphene oxide hybrids for catalytic and electrocatalytic reduction of CO_2. *Chem. Eur. J.* **2020**, *26*, 8801–8809. [CrossRef]
30. Zhang, C.; Yang, S.; Wu, J.; Liu, M.; Yazdi, S.; Ren, M.; Sha, J.; Zhong, J.; Nie, K.; Jalilov, A.S.; et al. Electrochemical CO_2 reduction with atomic iron-dispersed on nitrogen-doped graphene. *Adv. Energy Mater.* **2018**, *8*, 1703487. [CrossRef]
31. Sreekanth, N.; Nazrulla, M.A.; Vineesh, T.V.; Sailaja, K.; Phani, K.L. Metal-free boron-doped graphene for selective electroreduction of carbon dioxide to formic acid/formate. *Chem. Commun.* **2015**, *51*, 16061–16064. [CrossRef]
32. Wang, H.; Chen, Y.; Hou, X.; Ma, C.; Tan, T. Nitrogen-doped graphenes as efficient electrocatalysts for the selective reduction of carbon dioxide to formate in aqueous solution. *Green Chem.* **2016**, *18*, 3250–3256. [CrossRef]
33. Han, P.; Yu, X.; Yuan, D.; Kuang, M.; Wang, Y.; Al-Enizi, A.M.; Zheng, G. Defective graphene for electrocatalytic CO_2 reduction. *J. Colloid Interface Sci.* **2019**, *534*, 332–337. [CrossRef] [PubMed]
34. Jiang, K.; Siahrostami, S.; Zheng, T.; Hu, Y.; Hwang, S.; Stavitski, E.; Peng, Y.; Dynes, J.; Gangisetty, M.; Su, D.; et al. Isolated Ni single atoms in graphene nanosheets for high-performance CO_2 reduction. *Energy Environ. Sci.* **2018**, *11*, 893–903. [CrossRef]
35. Sekar, P.; Calvillo, L.; Tubaro, C.; Baron, M.; Pokle, A.; Carraro, F.; Martucci, A.; Agnoli, S. Cobalt spinel nanocubes on N-doped graphene: A synergistic hybrid electrocatalyst for the highly selective reduction of carbon dioxide to formic acid. *ACS Catal.* **2017**, *7*, 7695–7703. [CrossRef]
36. Ma, T.; Fan, Q.; Li, X.; Qiu, J.; Wu, T.; Sun, Z. Graphene-based materials for electrochemical CO_2 reduction. *J. CO_2 Util.* **2019**, *30*, 168–182. [CrossRef]
37. Ma, Z.; Tsounis, C.; Kumar, P.V.; Han, Z.; Wong, R.J.; Toe, C.Y.; Zhou, S.; Bedford, N.M.; Thomsen, L.; Ng, Y.H.; et al. Enhanced electrochemical CO_2 reduction of Cu@Cu_xO nanoparticles decorated on 3D vertical graphene with intrinsic sp3-type defect. *Adv. Funct. Mater.* **2020**, *30*, 1910118. [CrossRef]
38. Fazel Zarandi, R.; Rezaei, B.; Ghaziaskar, H.; Ensafi, A. Modification of copper electrode with copper nanoparticles@reduced graphene oxide–Nile blue and its application in electrochemical CO_2 conversion. *Mater. Today Energy* **2020**, *18*, 100507. [CrossRef]
39. Yuan, J.; Yang, M.P.; Zhi, W.Y.; Wang, H.; Wang, H.; Lu, J.X. Efficient electrochemical reduction of CO_2 to ethanol on Cu nanoparticles decorated on N-doped graphene oxide catalysts. *J. CO_2 Util.* **2019**, *33*, 452–460. [CrossRef]
40. Ni, W.; Li, C.; Zang, X.; Xu, M.; Huo, S.; Liu, M.; Yang, Z.; Yan, Y.M. Efficient electrocatalytic reduction of CO_2 on Cu_xO decorated graphene oxides: An insight into the role of multivalent Cu in selectivity and durability. *Appl. Catal. B* **2019**, *259*, 118044. [CrossRef]

41. Dongare, S.; Singh, N.; Bhunia, H. Nitrogen-doped graphene supported copper nanoparticles for electrochemical reduction of CO_2. *J. CO_2 Util.* **2021**, *44*, 101382. [CrossRef]
42. Zhu, G.; Li, Y.; Zhu, H.; Su, H.; Chan, S.H.; Sun, Q. Enhanced CO_2 electroreduction on armchair graphene nanoribbons edge-decorated with copper. *Nano Res.* **2021**, *10*, 1641–1650. [CrossRef]
43. Li, Q.; Zhu, W.; Fu, J.; Zhang, H.; Wu, G.; Sun, S. Controlled assembly of Cu nanoparticles on pyridinic-N rich graphene for electrochemical reduction of CO_2 to ethylene. *Nano Energy* **2016**, *24*, 1–9. [CrossRef]
44. Yuan, J.; Yang, M.P.; Hu, Q.L.; Li, S.M.; Wang, H.; Lu, J.X. Cu/TiO_2 nanoparticles modified nitrogen-doped graphene as a highly efficient catalyst for the selective electroreduction of CO_2 to different alcohols. *J. CO_2 Util.* **2018**, *24*, 334–340. [CrossRef]
45. Geioushy, R.; Khaled, M.; Alhooshani, K.; Hakeem, A.; Rinaldi, A. Graphene/ZnO/Cu_2O electrocatalyst for selective conversion of CO_2 into n-propanol. *Electrochim. Acta* **2017**, *245*, 448–454. [CrossRef]
46. Song, Y.; Peng, R.; Hensley, D.K.; Bonnesen, P.V.; Liang, L.; Wu, Z.; Meyer, H.M., III; Chi, M.; Ma, C.; Sumpter, B.G.; et al. High-Selectivity Electrochemical Conversion of CO_2 to Ethanol using a Copper Nanoparticle/N-Doped Graphene Electrode. *ChemistrySelect* **2016**, *1*, 6055–6061. [CrossRef]
47. Cao, C.; Wen, Z. Cu nanoparticles decorating rGO nanohybrids as electrocatalyst toward CO_2 reduction. *J. CO_2 Util.* **2017**, *22*, 231–237. [CrossRef]
48. Hossain, M.N.; Wen, J.; Chen, A. Unique copper and reduced graphene oxide nanocomposite toward the efficient electrochemical reduction of carbon dioxide. *Sci. Rep.* **2017**, *7*, 3184. [CrossRef]
49. Geioushy, R.; Khaled, M.M.; Hakeem, A.S.; Alhooshani, K.; Basheer, C. High efficiency graphene/Cu_2O electrode for the electrochemical reduction of carbon dioxide to ethanol. *J. Electroanal. Chem.* **2017**, *785*, 138–143. [CrossRef]
50. Liu, S.; Huang, S. Structure engineering of Cu-based nanoparticles for electrochemical reduction of CO_2. *J. Catal.* **2019**, *375*, 234–241. [CrossRef]
51. Legrand, U.; Boudreault, R.; Meunier, J. Decoration of N-functionalized graphene nanoflakes with copper-based nanoparticles for high selectivity CO_2 electroreduction towards formate. *Electrochim. Acta* **2019**, *318*, 142–150. [CrossRef]
52. Dai, L. Functionalization of graphene for efficient energy conversion and storage. *Acc. Chem. Res.* **2013**, *46*, 31–42. [CrossRef] [PubMed]
53. Wang, H.; Yuan, X.; Zeng, G.; Wu, Y.; Liu, Y.; Jiang, Q.; Gu, S. Three dimensional graphene based materials: Synthesis and applications from energy storage and conversion to electrochemical sensor and environmental remediation. *Adv. Colloid Interface Sci.* **2015**, *221*, 41–59. [CrossRef] [PubMed]
54. Siahrostami, S.; Jiang, K.; Karamad, M.; Chan, K.; Wang, H.; Nørskov, J. Theoretical investigations into defected graphene for electrochemical reduction of CO_2. *ACS Sustain. Chem. Eng.* **2017**, *5*, 11080–11085. [CrossRef]
55. Varela, A.S.; Ranjbar Sahraie, N.; Steinberg, J.; Ju, W.; Oh, H.S.; Strasser, P. Metal-doped nitrogenated carbon as an efficient catalyst for direct CO_2 electroreduction to CO and hydrocarbons. *Angew. Chem. Int. Ed.* **2015**, *54*, 10758–10762. [CrossRef]
56. Cheng, M.J.; Kwon, Y.; Head-Gordon, M.; Bell, A.T. Tailoring metal-porphyrin-like active sites on graphene to improve the efficiency and selectivity of electrochemical CO_2 reduction. *J. Phys. Chem. C* **2015**, *119*, 21345–21352. [CrossRef]
57. Pérez-Sequera, A.C.; Díaz-Pérez, M.A.; Serrano-Ruiz, J.C. Recent advances in the electroreduction of CO_2 over heteroatom-doped carbon materials. *Catalysts* **2020**, *10*, 1179. [CrossRef]
58. Yang, N.; Waldvogel, S.R.; Jiang, X. Electrochemistry of carbon dioxide on carbon electrodes. *ACS Appl. Mater. Interfaces* **2016**, *8*, 28357–28371. [CrossRef]
59. Liu, J.; Song, P.; Ning, Z.; Xu, W. Recent advances in heteroatom-doped metal-free electrocatalysts for highly efficient oxygen reduction reaction. *Electrocatalysis* **2015**, *6*, 132–147. [CrossRef]
60. Wong, W.; Daud, W.; Mohamad, A.; Kadhum, A.; Loh, K.; Majlan, E. Recent progress in nitrogen-doped carbon and its composites as electrocatalysts for fuel cell applications. *Int. J. Hydrogen. Energy* **2013**, *38*, 9370–9386. [CrossRef]
61. Li, W.; Seredych, M.; Rodríguez-Castellón, E.; Bandosz, T.J. Metal-free nanoporous carbon as a catalyst for electrochemical reduction of CO_2 to CO and CH_4. *ChemSusChem* **2016**, *9*, 606–616. [CrossRef]
62. Terrones, H.; Lv, R.; Terrones, M.; Dresselhaus, M.S. The role of defects and doping in 2D graphene sheets and 1D nanoribbons. *Rep. Prog. Phys.* **2012**, *75*, 062501, [CrossRef] [PubMed]
63. Sharma, P.P.; Wu, J.; Yadav, R.M.; Liu, M.; Wright, C.J.; Tiwary, C.S.; Yakobson, B.I.; Lou, J.; Ajayan, P.M.; Zhou, X.D. Nitrogen-doped carbon nanotube arrays for high-efficiency electrochemical reduction of CO_2: On the understanding of defects, defect density, and selectivity. *Angew. Chem. Int. Ed.* **2015**, *54*, 13701–13705. [CrossRef] [PubMed]
64. Chai, G.L.; Guo, Z.X. Highly effective sites and selectivity of nitrogen-doped graphene/CNT catalysts for CO_2 electrochemical reduction. *Chem. Sci.* **2016**, *7*, 1268–1275. [CrossRef] [PubMed]
65. Liu, Y.; Chen, S.; Quan, X.; Yu, H. Efficient electrochemical reduction of carbon dioxide to acetate on nitrogen-doped nanodiamond. *J. Am. Chem. Soc.* **2015**, *137*, 11631–11636. [CrossRef] [PubMed]
66. Wu, J.; Yadav, R.M.; Liu, M.; Sharma, P.P.; Tiwary, C.S.; Ma, L.; Zou, X.; Zhou, X.D.; Yakobson, B.I.; Lou, J.; et al. Achieving highly efficient, selective, and stable CO_2 reduction on nitrogen-doped carbon nanotubes. *ACS Nano* **2015**, *9*, 5364–5371. [CrossRef] [PubMed]
67. Schouten, K.J.P.; Kwon, Y.; van der Ham, C.J.M.; Qin, Z.; Koper, M.T.M. A new mechanism for the selectivity to C1 and C2 species in the electrochemical reduction of carbon dioxide on copper electrodes. *Chem. Sci.* **2011**, *2*, 1902–1909. [CrossRef]
68. Schouten, K.J.P.; Qin, Z.; Pérez Gallent, E.; Koper, M.T.M. Two pathways for the formation of ethylene in CO reduction on single-crystal copper electrodes. *J. Am. Chem. Soc.* **2012**, *134*, 9864–9867. [CrossRef]

69. Hori, Y.; Murata, A.; Takahashi, R.; Suzuki, S. Electroreduction of carbon monoxide to methane and ethylene at a copper electrode in aqueous solutions at ambient temperature and pressure. *J. Am. Chem. Soc.* **1987**, *109*, 5022–5023. [CrossRef]
70. Back, S.; Lim, J.; Kim, N.Y.; Kim, Y.H.; Jung, Y. Single-atom catalysts for CO_2 electroreduction with significant activity and selectivity improvements. *Chem. Sci.* **2017**, *8*, 1090–1096. [CrossRef]
71. Heyd, J.; Scuseria, G.E.; Ernzerhof, M. Hybrid functionals based on a screened Coulomb potential. *J. Chem. Phys.* **2003**, *118*, 8207–8215. [CrossRef]
72. Krukau, A.V.; Vydrov, O.A.; Izmaylov, A.F.; Scuseria, G.E. Influence of the exchange screening parameter on the performance of screened hybrid functionals. *J. Chem. Phys.* **2006**, *125*, 224106. [CrossRef]
73. Dovesi, R.; Saunders, V.R.; Roetti, C.; Orlando, R.; Zicovich-Wilson, C.M.; Pascale, F.; Civalleri, B.; Doll, K.; Harrison, N.M.; Bush, I.J.; et al. *CRYSTAL17 User's Manual*; University of Torino: Torino, Italy, 2017.
74. Peintinger, M.F.; Oliveira, D.V.; Bredow, T. Consistent Gaussian basis sets of triple-zeta valence with polarization quality for solid-state calculations. *J. Comput. Chem.* **2013**, *34*, 451–459. [CrossRef]
75. Gatti, C.; Saunders, V.R.; Roetti, C. Crystal field effects on the topological properties of the electron density in molecular crystals: The case of urea. *J. Chem. Phys.* **1994**, *101*, 10686–10696. [CrossRef]
76. Monkhorst, H.J.; Pack, J.D. Special points for Brillouin-zone integrations. *Phys. Rev. B* **1976**, *13*, 5188–5192. [CrossRef]
77. Usseinov, A.B.; Akilbekov, A.T.; Kotomin, E.A.; Popov, A.I.; Seitov, D.D.; Nekrasov, K.A.; Giniyatova, S.G.; Karipbayev, Z.T. The first principles calculations of CO_2 adsorption on $(10\bar{1}0)$ ZnO surface. *AIP Conf. Proc.* **2019**, *2174*, 020181. [CrossRef]
78. Norsko, J. Chemisorption on metal surfaces. *Rep. Prog. Phys.* **1990**, *53*, 1253. [CrossRef]
79. Li, C.; Ciston, J.; Kanan, M. Electroreduction of carbon monoxide to liquid fuel on oxide-derived nanocrystalline copper. *Nature* **2014**, *508*, 504–507. [CrossRef]
80. Feng, X.; Jiang, K.; Fan, S.; Kanan, M.W. A direct grain-boundary-activity correlation for CO electroreduction on Cu nanoparticles. *ACS Cent. Sci.* **2016**, *2*, 169–174. [CrossRef]
81. Cheng, T.; Xiao, H.; Goddard, W.A. Nature of the active sites for CO reduction on copper nanoparticles; suggestions for optimizing performance. *J. Am. Chem. Soc.* **2017**, *139*, 11642–11645. [CrossRef]